Pure appl. geophys. 151 (1998) 17–45
0033–4553/98/010017–29 $ 1.50 + 0.20/0

Pure and Applied Geophysics

Elastic Kirchhoff-Helmholtz Synthetic Seismograms*

ALEXANDER DRUZHININ,[1] HELLE PEDERSEN,[2] MICHEL CAMPILLO[2] and WOOHAN KIM[3]

Abstract—An approximate hybrid formulation of the elastic Kirchhoff-Helmholtz theory for numerical simulation of seismic wave propagation in multilayered inhomogeneous and transversely isotropic media is developed. The layer boundaries can be curved or irregular. We insert a general computational ansatz into the basic elastodynamic divergence theorem to express the unknown variables in terms of slowly varying amplitude and phase functions. In situations where the geometrical optics approximation becomes invalid, more accurate methods can be applied to compute these functions. In particular, the kernel remains regular when rays have caustics on the target integral surface. Branch points are taken into account to include head waves. Both elementary solutions and WKBJ expansion are employed to compute the Green's function. To reduce the resulting integral to a numerical form, the surface is divided into a set of segments and the above functions are replaced by their local polynomial series in the vicinity of each segment. It allows us to construct an error-predictive numerical algorithm in which the truncation error is prescribed via the higher order terms of such series. We show, using geologically relevant synthetic models, the performance of the proposed technique.

Key words: Synthetic seismograms, elastic waves, Kirchhoff, Green's function, inhomogeneity, anisotropy, hybrid.

1. Introduction

The Kirchhoff-Helmholtz (KH) theory provides a powerful tool to create a combined generalization of existing asymptotic and numerical methods to solve many wave propagation problems involving heterogeneous and anisotropic media (for an extensive review of the KH theory, cf. FRAZER and SEN, 1985; TYGEL *et al.*, 1994). In most KH techniques, the kernel of the KH integral is constructed upon use of the Asymptotic Ray Theory (ART) (ČERVENÝ and RAVINDRA, 1971; ČERVENÝ *et al.*, 1977). Therefore, well-known validity conditions of the ART (ČERVENÝ *et al.*, 1977; BEN-MENAHEM and BEYDOUN, 1985; FRADKIN, 1989;

[1] Institute for Solid Earth Physics, University of Bergen, Allégaten 41, N5007 Bergen, Norway.
[2] IRIGM, Université Joseph Fourier, BP 53X, 38041 Grenoble, Cedex, France.
[3] Department of Geology, Gyeongsang National Univeristy, Gazwa-Dong 900, Chinju 660-701, South Korea.

* Paper presented at the EAGE 59th Conference and Technical Exhibition—Geneva, Switzerland, 26–30 May 1997—Geophysical Division (Papers E015, E016).

KRAVTSOV and ORLOV, 1993) have to be taken into account in the ray-Kirchhoff algorithms.

This problem can be solved by using a more accurate approximation of the KH integrand, based on the exact ray theory (ZHU, 1988; FOREMAN, 1989; DRUZHININ, 1994) or the complex continued ART Green's function (FELSEN, 1984; WU, 1985). Their extension was proposed in the Method of the Interference Integral (MII) (KRAVTSOV and ORLOV, 1993). Another approach is based upon the additional decomposition of the integrand to derive a multi-folded extension of the KH theory (BOSTRÖM, 1980; KENNETT, 1984; FRAZER and SEN, 1985; WENZEL *et al.*, 1990).

Even in these improved forms, KH integrals have been infrequently used in seismic modelling. The reason is two-fold: (1) it is rather difficult to calculate these integrals numerically although many advanced quadrature algorithms have been proposed (PIESSENS *et al.*, 1983; STAMNES *et al.*, 1983; FRAZER, 1988; HAIGER and LIU, 1992); (2) all the relevant aspects of the wave field can be accurately treated by the theory of Huygens' principle if and only if the corresponding Green's function is known (PAO and VARATHARAJULU, 1976). Thus, the main problem is to find such function or suitable approximation, and to develop a fast and robust quadrature formula for the numerical computation of the resulting path integral. Otherwise, the finite-difference or finite-element methods for solving partial differential equations of wave motion should be applied as exclusive tools for calculating the complete solution to these equations.

ROBERTS (1994) and DRUZHININ (1994) have attempted to solve this problem independently by using the general Green's function computational ansatz to combine the existing asymptotic and fast numerical techniques for optimizing the advantages of each without use of diffracted ray tracing. However, DRUZHININ (1994) considered only the simple scalar KH formula and second-order polynomial approximations (following STAMNES *et al.*, 1983). Full advantage was therefore not taken of the Green's function computations and development of the error-predictive numerical algorithm.

The present paper attempts to remove such shortcomings. By analogy with the MII, we derive the elastic KH formula without limitations to the wave code and to the method of computing Green's function. Next, we modify the above numerical algorithm to calculate the final oscillatory integral by minimization of the overall truncation error.

2. Theoretical Background

In this section we briefly summarize the crucial points of our KH technique that are needed in the practical computations to follow. We furthermore concentrate on the elastic case. Many features of the formalism presented below are also expected to be valid in the anelastic case.

2.1 Basic Integral Theorem

We begin with the explicit elastodynamic divergence theorem for steady-state waves (PAO and VARATHARAJULU, 1976)

$$u_m(\mathbf{x}) = \int_\Sigma n'_j B_{ijkl}(\mathbf{x}')[g_{im}(\mathbf{x}, \mathbf{x}')\partial'_k u_l^+(\mathbf{x}') - u_i^+(\mathbf{x}')\partial'_k g_{lm}(\mathbf{x}, \mathbf{x}')]\, ds' \tag{1}$$

where $u_m(\mathbf{x})$ is the mth component of displacement vector at observation point $\mathbf{x}$ within a domain V with boundary $\partial V = \Sigma \cup \Sigma_\infty$ occupied by an elastic medium, B_{ijkl} are the components of the 4th order elastic tensor inside V, ∂'_k is the spatial derivative with respect to coordinates x'_k of the current point $\mathbf{x}'$ of the target interface Σ, ds' is an infinitesimal area element at $\mathbf{x}'$ on Σ, n'_j is the jth component of unit outward normal to Σ at $\mathbf{x}'$ (the indices i, j, k, l, m take values 1, 2 and 3; summation rule over repeated indices is understood throughout). Equation (1) establishes the basic integral relation between the displacement vector $\mathbf{u}$ as a function of $\mathbf{x}$ and its boundary value $\mathbf{u}^+$ at $\mathbf{x}'$ from the inside of volume V. The term $g_{mi}(\mathbf{x}, \mathbf{x}')$ is known as the full-space Green's tensor within V that represents the displacement in mth direction at $\mathbf{x}$ due to a concentrated body force applied at the point $\mathbf{x}'$ in the direction of the coordinate x_i. Assuming the radiation conditions on Σ_∞ (PAO and VARATHARAJULU, 1976), zero initial conditions and no body forces inside V, the above equation can be used to study the scattering effect by Σ. It is worthwhile to remind that the radiation conditions are imposed on the behavior of the displacement and traction vectors at infinity. They imply that the energy flux at infinity should be in the outward direction.

The boundary wave field in eq. (1) is decomposed in the form (ROBERTS, 1994; DRUZHININ, 1994)

$$\mathbf{u}^+ = \sum_{p=1}^{P} \mathbf{u}_p^+ \tag{2}$$

in terms of the components

$$\mathbf{u}_p^+(\mathbf{x}', \omega) = \mathbf{U}_p^+(\mathbf{x}', \omega) \exp[i\omega\tau_p(\mathbf{x}', \omega)] \tag{3}$$

where ω is the circular frequency, $\mathbf{U}_p^+$ are amplitude functions, and τ_p are corresponding phase functions determined formally from the differential equations of exact ray theory (ZHU, 1988; FOREMAN, 1989; DRUZHININ, 1994). The index $p = 1, 2, \ldots, P$ refers to different arrivals of various elementary waves, such as primary and multiply reflections, converted waves, etc. (there is no summation over indices in eq. (3)). By analogy with the ART theory, each elementary wave in the form (3) deals with a fixed ray code δ_p at a time (ČERVENÝ and RAVINDRA, 1971; ČERVENÝ *et al.*, 1977). Besides, the terms (3) can also be regarded as a set of basis functions to gain advantage of the method of wave superposition (BOSTRÖM, 1980; KOOPMAN *et al.*, 1989).

Inserting (2) and (3) into (1), the fundamental integral then becomes

$$\mathbf{u} = \sum_{p=1}^{P} \mathbf{u}_p \tag{4}$$

with terms

$$u_{mp}(\mathbf{x}) = \int_{\Sigma} n'_j B_{ijkl}(\mathbf{x}') \{ g_{im}(\mathbf{x}, \mathbf{x}') u^+_{lp}(\mathbf{x}') [\partial'_k \ln U^+_{lp}(\mathbf{x}') + i\omega p^+_{kp}(\mathbf{x}')] - u^+_{ip}(\mathbf{x}') \partial'_k g_{lm}(\mathbf{x}, \mathbf{x}') \} \, ds' \tag{5}$$

where $p^+_{kp} = \partial'_k \tau^+_p(\mathbf{x}')$ is the kth slowness component of the elementary wave (3) after its propagation across Σ, according to the wave code δ_p (in eq. (5), there is no summation over indices m and p). The physical meaning of eq. (4) is an interference of the scattered wave fields at $\mathbf{x}$ (cf. eq. (5)) generated by the elementary waves at Σ given by solution (3).

Using the appropriate boundary conditions, we write (cf. DRUZHININ, 1994)

$$U^+_{lp}(\mathbf{x}') = K(\mathbf{x}'; \delta_p) U_{lp}(\mathbf{x}'), \quad p^+_{kp} = \Pi_{kj}(\mathbf{x}'; \delta_p) \, p_{jp} \tag{6}$$

where $U_{lp}(\mathbf{x}')$ and $p_{jp} = \partial'_j \tau_p(\mathbf{x}')$ are the amplitude and slowness vector components of incident wave field at $\mathbf{x}'$, $K(\mathbf{x}'; \delta_p)$ and $\Pi_{kj}(\mathbf{x}'; \delta_p)$ are the reflection/transmission coefficient and the propagator matrix specified by the wave code δ_p. In the case where the amplitudes in eq. (3) are determined in the ART approximation, eq. (6) should be replaced by the ordinary plane-wave reflection formulae and the Snell's propagator matrix (FRAZER and SEN, 1985). Such formulae are well-established for the stress-displacement continuity conditions in the media with arbitrary elastic layers as well as for the more general boundary conditions of the slip contact (DRUZHININ and LUNEVA, 1993). A correction for the anelasticity can be introduced upon the use of the ART (e.g., DRUZHININ, 1993).

2.2 The Green's Function

Equations (4–6) can only be used in types of media for which the Green's tensor is known. In general, we cannot analytically determine the Green's tensor for arbitary elastic or anelastic media. However, a familiar Green's dyadic eigenvector expansion can be employed (e.g., DRUZHININ and CAMPILLO, 1996)

$$g_{im} = \sum_{\mu=1}^{M} \left[g^{(\mu\mu)} e^{(\mu)}_i e^{(\mu)}_m + \frac{1}{i\omega} \sum_{\nu=1}^{M} g^{(\mu\nu)} e^{(\mu)}_i e^{(\nu)}_m \right], \quad \nu \neq \mu, \tag{7}$$

$$g^{(\mu\nu)} = G^{(\mu\nu)} \exp(\mathrm{i}\omega\tau^{(\mu\nu)}), \quad \mu, \nu = 1, 3, \ldots, M \tag{8}$$

by summation over different arrivals of M elementary wave modes of the magnitudes (8). Here, the polarizations $\mathbf{e}^{(\mu)}$ represent solutions of the Christoffel equation (e.g., ČERVENÝ *et al.*, 1977). In the case of a full-space Green's tensor, the indices

$\mu, \nu = 1, 2, 3$ refer to three wave types corresponding to one quasi-P and two quasi-transverse qS1 and qS2 wave motions (BEN-MENAHEM 1990; BEN-MENAHEM and SENA, 1990; DONG and SCHMITT, 1994). In the ART approximation (ČERVENÝ *et al.*, 1977; DRUZHININ, 1993), the amplitude $G^{(\mu\nu)}$ and phase $\tau^{(\mu\nu)}$ functions in (8) can be determined from the corresponding equations for the main and additional components of the wave field. According to the exact ray theory (ZHU, 1988; FOREMAN, 1989; DRUZHININ, 1994), these functions can be frequency-dependent and may give rise to a very useful frequency-dependent ray diagram near the edges, caustics, etc. In the regular domains of the ray field, the diagonal ($\nu = \mu$) components (8) account for the energy transport along the ray tube of the considered wave mode. Other components are due to the *coupling* effect caused by the interaction between the ray tubes of different wave types.

2.3 KH Formula

Inserting (7) and (8) into (5) and changing the orders of summation and integration, we find

$$u_m = \sum_{p=1}^{P} \sum_{\mu=1}^{M} \left(u_{mp\mu} + \Delta u_{mp\mu\mu} + \sum_{\nu=1}^{M} \Delta u_{mp\mu\nu} \right), \quad \nu \neq \mu \tag{9}$$

with

$$u_{mp\mu}(\mathbf{x}) = i\omega \int_{\Sigma} n'_j B_{ijkl}(\mathbf{x}') g^{(\mu\mu)}(\mathbf{x}, \mathbf{x}') u_p^+(\mathbf{x}') \phi^{(\mu)}_{imlkp}(\mathbf{x}, \mathbf{x}')\, ds' \tag{10}$$

where

$$\phi^{(\mu)}_{imlkp} = e_m^{(\mu)} (e_i^{(\mu)} e_{lp}^+ p_{kp}^+ - e_l^{(\mu)} e_{ip}^+ p_{k\mu\mu}), \tag{11}$$

and $u_p^+ = (\mathbf{u}_p^+ \cdot \mathbf{e}_p^+)$ is the scalar product of eq. (3) and the unit polarization vector $\mathbf{e}_p^+ = \mathbf{U}_p^+ / U_p^+$ from (3) with components e_{lp}^+, $p_{k\mu\nu} = \partial'_k \tau^{(\mu\nu)}$ is the kth component of the slowness vector orthogonal to the phase surface $\tau^{(\mu\nu)} = t$ ($\mu, \nu = 1, 2, 3$). The additional terms in eq. (9) are

$$\Delta u_{mp\mu\nu}(\mathbf{x}) = \int_{\Sigma} n'_j B_{ijkl}(\mathbf{x}') g^{(\mu\nu)}(\mathbf{x}, \mathbf{x}') u_p^+(\mathbf{x}') \Delta\phi^{(\mu\nu)}_{imlkp}(\mathbf{x}, \mathbf{x}')\, ds', \ \mu, \nu = 1, 2, 3$$

where

$$\begin{aligned} \Delta\phi^{(\mu\nu)}_{imlkp} = (i\omega)^{-\delta} e_i^{(\mu)} e_m^{(\nu)} e_{lp}^+ (\partial'_k \ln U_{lp}^+ + \delta i\omega p_{kp}^+) \\ - e_{ip}^+ [\delta p_{k\mu\nu} e_l^{(\mu)} e_m^{(\nu)} + (i\omega)^{-\delta} (e_l^{(\mu)} e_m^{(\nu)} \partial'_k \ln G^{(\mu\nu)} + \partial'_k (e_l^{(\mu)} e_m^{(\nu)}))] \end{aligned}$$

$$\delta = \begin{cases} 0 & \text{for } \nu = \mu \\ 1 & \text{for } \nu \neq \mu \end{cases}$$

In the framework of the KH theory, eq. (9) can be interpreted as a continuous superposition of the secondary waves spreading from the points of contour Σ. One example of eq. (9) is a scalar ($\mu = \nu = 1$) normal mode representation of the point source wave field in a waveguide with some mode cutoff P (FOREMAN, 1989). Correction of eq. (10) for the head-wave arrivals is discussed in Appendix A.

It should be emphasized that no approximations have been made in the development so far. However, the high-frequency condition

$$\omega/\omega_c \gg 1 \tag{12}$$

with a cut-off frequency ω_c is often imposed (BEN-MENAHEM and BEYDOUN, 1985). The parameter ω_c is assumed to be contained in the range $\omega_1 < \omega < \omega_2$, where ω_2 is the Nyquist critical frequency, and ω_1 can be expressed in terms of the transverse size of the Fresnel volume (KRAVTSOV and ORLOV, 1993) or the scale of a model irregularity (ČERVENÝ *et al.*, 1977; FRADKIN, 1989).

Condition (12), in turn, implies that (DRUZHININ, 1994)

$$\omega|(\mathbf{n}' \cdot \mathbf{p}_p^+)| \gg |(\mathbf{n}' \cdot \nabla' \ln U_{lp}^+)| \tag{13}$$

and, similarly,

$$\omega|(\mathbf{n}' \cdot \mathbf{p}_{\mu\nu})| \gg |(\mathbf{n}' \cdot \nabla' \ln G^{(\mu\nu)})| \tag{14}$$

for $p = 1, \ldots, P$ and $l, \mu, \nu = 1, 2, 3$. Hence, ignoring above additional terms in eq. (9), we arrive at the surface KH integral (10). Without a loss of generality, a similar formula can also be obtained for the volume integral (LUMLEY and BEYDOUN, 1993). Equation (10) can be used when the surface Σ is discontinuous and/or when Σ and the receiver are located at an envelope (caustic) of the ray family associated with the source. Actually, the choice of Σ does not depend upon the problem considered because we have not yet specified how to compute the amplitude and phase functions in eqs. (3) and (8) as well as the coefficients in eq. (6). Note that these results contain the existing KH techniques as a special case (cf. Appendix B), and that it was the MII that provided the motivation for the results obtained herein. A well-known particular case of eq. (10) is the ray-Kirchhoff integral (e.g., HADDON and BUCHEN, 1981; SCOTT and HELMBERGER, 1983; FRAZER and SEN, 1985; GELIUS, 1993; TYGEL *et al.*, 1994) when the amplitudes $G^{(\mu\nu)}$ and U_{lp}^+ are determined in the ART approximation, so that conditions (13) and (14) take a form of the ordinary far-field validity conditions (BEN-MENAHEM and BEYDOUN, 1985; KRAVTSOV and ORLOV, 1993), and plane wave reflection/transmission coefficients are used. However, these integrals are invalid when rays have caustics on Σ (cf., ZHU, 1988). The more generic eq. (10) is intended to solve this problem.

2.4 Time-domain response

Let $f(t)$ is a source wavelet with a Fourier spectrum $F(\omega)$ that is regularly sampled. Then, the time-domain response can be constructed by taking a standard inverse FFT of eq. (9) with $F(\omega)$. However, the final algorithm would be rather time-consuming due to the frequency loop.

In terms of analytic signal $f_s(t) = f(t) + if^H(t)$ where $f^H(t)$ denotes the Hilbert transform of $f(t)$ (ČERVENÝ and RAVINDRA, 1971; ČERVENÝ *et al.*, 1977), the time-domain form of eq. (10) becomes

$$u_{mp\mu}(t) \sim \mathrm{Re} \int_\Sigma \Phi_{mp\mu}(\omega') f_s(t - \tau_{p\mu})\, ds'$$

$$= \int_\Sigma [\mathrm{Re}\, \Phi_{mp\mu}(\omega') f(t - \tau_{p\mu}) - Im \Phi_{mp\mu}(\omega') f^H(t - \tau_{p\mu})]\, ds' \qquad (15)$$

where ω' is the predominant frequency of spectrum $F(\omega)$. Here, the amplitude and phase functions are

$$\Phi_{mp\mu}(\mathbf{x}, \mathbf{x}'; \omega) = i\omega n'_j B_{ijkl}(\mathbf{x}') G^{(\mu\mu)}(\mathbf{x}, \mathbf{x}'; \omega) U_p^+(\mathbf{x}'; \omega) \phi^{(\mu)}_{imlkp}(\mathbf{x}, \mathbf{x}'; \omega), \qquad (16)$$

$$\tau_{p\mu}(\mathbf{x}, \mathbf{x}') = \tau^{(\mu\mu)}(\mathbf{x}, \mathbf{x}') + \tau_p(\mathbf{x}') \qquad (17)$$

with amplitude and phase terms from eqs. (3), (8) and (11). Thus, the synthetic seismograms can be constructed without invoking the use of Fourier synthesis. However, the applicability of eq. (15) is restricted by the band-limited spectrum $F(\omega)$. Consequently, this operation cannot be exactly accomplished without introducing instabilities which were studied numerically (DRUZHININ and CAMPILLO, 1996). To avoid the instabilities, we may employ an explicit form of the time-domain KH integral (HADDON and BUCHEN, 1981; DRUZHININ and KIM, 1995).

2.5 Numerical Formula

This subsection of the paper discusses procedural issues in the numerical evaluation of the KH integral (10). The additional terms of eq. (10) can be evaluated similarly, but the algorithm becomes rather lengthy because of the more complicated integrand. By means of conditions (12), (13) and (14) these complicated terms can be eliminated.

To reduce the KH integral (10) to a numerical form, the surface Σ is divided into N segments $\Delta\Sigma_n$ and the area of each segment is represented by Δs_n. Dropping the indices m, p and μ, eq. (10) can be rewritten in the form

$$u(\mathbf{x}) = \sum_{n=1}^{N} \Delta u(\mathbf{x}, \mathbf{x}'_n) \qquad (18)$$

with

$$\Delta u(\mathbf{x}, \mathbf{x}'_n) = \Delta u^{(0)}(\mathbf{x}, \mathbf{x}'_n)\Delta I_n, \tag{19}$$

$$\Delta u^{(0)}(\mathbf{x}, \mathbf{x}'_n) = u(\mathbf{x}, \mathbf{x}'_n)\Delta s_n, \tag{20}$$

$$\Delta I_n = \frac{1}{\Delta s_n}\int_{\Delta\Sigma_n} \Delta u_n(\mathbf{x}, \mathbf{x}')\, ds', \tag{21}$$

$$\Delta u_n(\mathbf{x}, \mathbf{x}') = u(\mathbf{x}, \mathbf{x}')/u(\mathbf{x}, \mathbf{x}'_n) = \bar{\Phi}_n(\mathbf{x}, \mathbf{x}') \exp[i\omega\Delta\tau_n(\mathbf{x}, \mathbf{x}')],$$

$$u(\mathbf{x}, \mathbf{x}') = \Phi(\mathbf{x}, \mathbf{x}') \exp[i\omega\tau(\mathbf{x}, \mathbf{x}')],$$

$$\bar{\Phi}_n(\mathbf{x}, \mathbf{x}') = \Phi(\mathbf{x}, \mathbf{x}')/\Phi(\mathbf{x}, \mathbf{x}'_n),\ \Delta\tau_n(\mathbf{x}, \mathbf{x}') = \tau(\mathbf{x}, \mathbf{x}') - \tau(\mathbf{x}, \mathbf{x}'_n),$$

where the amplitude Φ and phase functions τ are defined by eqs. (16) and (17), respectively, $\mathbf{x}'_n$ is a central point of the segment $\Delta\Sigma_n$. Equation (18) is also obtained by means of the wave superposition method (KOOPMAN *et al.*, 1989), including a source term corresponding to the elementary solution (3), applied to the region V, bounded by the surface ∂V, and combined with the boundary conditions (cf., eq. (6)). According to this interpretation, the segment $\Delta\Sigma_n$ acts as a secondary source generating wavelets after it has been struck by the incident wave given by eq. (3). These waves constitute the infinitesimal scattered wave fields expressed in terms of the KH integrand (20) and also some weighting factor or directivity function (21). If Δs_n for all $n = 1, 2, \ldots, N$ is made to be sufficiently small, the integrand in eq. (20) can be fixed at $\mathbf{x}'_n$ to get the simplest (rectangular) quadrature formula in which $\Delta I_n = 1$. Many fast numerical integration techniques apply this type of formula (e.g., WU, 1985; KOOPMAN *et al.*, 1989). Other techniques are the adaptive rectangular formula by HAIGER and LIU (1992), generalized Filon's method (FRAZER, 1988), second-order quadrature by STAMNES *et al.* (1983), etc. Our primary purpose here is to define the weight function (21) so as to provide a more accurate and stable evaluation of eq. (18) on the number N of segments.

For the sake of simplicity, we restrict ourselves to the 2D problem so that any point $\mathbf{x}'$ in Σ is specified by an arclength s. A central point $\mathbf{x}'_n$ on the nth segment $\Delta\Sigma_n$ has an arclength $s_n^0 = s_n + \Delta s_n/2$. We assume that the phase and amplitude functions in eq. (21) are sufficiently smooth functions of s which have a compact support in $(-\infty, \infty)$. Hence, we define their local Taylor expansions in the vicinity of $\mathbf{x}'_n$ (DRUZHININ and CAMPILLO, 1996)

$$\Delta\tau_n = \sum_{k=1}^{K} \tau_n^{(k)} t^k + O(t^{K+1}) \tag{22}$$

and, similarly,

$$\bar{\Phi}_n = 1 + \sum_{l=1}^{L} \Phi_n^{(l)} t^l + O(t^{L+1}) \tag{23}$$

with respect to the variable $t = (s - s_n^0)/\Delta s_n$. Instead of numerical formulae (STAMNES *et al.*, 1983), we can explicitly determine the coefficients

$$\tau_n^{(k)} = \frac{1}{k!}\frac{\partial^k \tau_n}{\partial t^k}\bigg|_{t=0} \quad \text{and} \quad \Phi_n^{(l)} = \frac{1}{l!}\frac{\partial^l \overline{\Phi_n}}{\partial t^l}\bigg|_{t=0}$$

if we consider a simpler problem for which closed-form scalar solutions such as (8) are available (e.g., BEN-MENAHEM, 1990). Consequently, the computations of the above coefficients are tedious but completely straightforward. Practically, we need to use the zero-order term of the series (23) only, since the amplitude (16) is normally a slowly varying function of t (DRUZHININ, 1994). By slowly varying, we mean that the length of the variations normalized on the wavlength λ_n of the waves under consideration at $\mathbf{x}_n'$ is much greater than the parameter $\varepsilon_n = \Delta s_n/\lambda_n$ (FRADKIN, 1989; KRAVTSOV and ORLOV, 1993). However, the most complete phase expansion (22) should be considered because of the high-frequency condition (12).

Inserting (22) and (23) into (21), changing integration variables in eq. (21) from s to t and noting that $\Phi_n^{(0)} = 1$ yields

$$\Delta I_n \sim I_n^{(L,K)} = \sum_{l=0}^{L} \Phi_n^{(l)} J_n^{(l,K)} \tag{24}$$

with

$$J_n^{(l,K)} = \int_{x^-}^{x^+} t^l \exp\left(i\omega \sum_{k=1}^{K} \tau_n^{(k)} t^k\right) dt \tag{25}$$

where

$$[x^-, x^+] = \begin{cases} [-0.5, +0.5] & 2 \le n \le N-1 \\ [-1.0, +0.5] & \text{for } n = 1 \\ [+0.5, +1.0] & n = N \end{cases}.$$

Thus, we obtain the polynomial expansion (24) of eq. (21), involving the family of special functions (25) well-established in the asymptotic diffraction theory (HANYGA, 1993; KRAVTSOV and ORLOV, 1993). These functions can be tabulated by the use of numerical algorithms reviewed by KRAVTSOV and ORLOV (1993) or with the QUADPACK subroutines (PIESSENS *et al.*, 1983). Even though they can be expressed explicitly in terms of the simple special functions only if $K \leqslant 2$ (STAMNES *et al.*, 1983), such an approximation provides a desirable freedom for the computation of eq. (18) since we do not specify K and L. Whenever the coefficients of the series (22) and (23) are known, it is possible to determine accurately the directivity function (21) uniformly over the grid $\{\mathbf{x}_n'\}$ when the condition $\varepsilon_n \ll 1$ of a small nth segment is not invoked. After computing the higher-order terms (25), we can construct an error-predictive numerical algorithm to compute the function (21) (Fig. 1). However, the suitability of the approximation (24) strongly depends upon the convergence properties of above series. In practice, we shall be content with results of the first few orders ($K \leqslant 3$).

2.6 Truncation Error

The error in eq. (18) resulting from the truncation of series (22) and (23) must be analyzed in detail. The main problem is to estimate the truncation error associated with the Kth order phase approximation (22). This error is defined by

$$\varepsilon_n^K = \max_{0 \leqslant l \leqslant L} \{\varepsilon_{nl}^K\}, \; \varepsilon_{nl}^K = \left| J_n^{(l,K+1)} - J_n^{(l,K)} \right| \tag{26}$$

or, by taking into account the first-order estimate

$$\exp(i\omega\tau_n^{(K+1)} t^{(K+1)}) - 1 = i\omega\tau_n^{(K+1)} t^{(K+1)} + O(\omega^2 t^{2(K+1)}),$$

for $\omega|\tau_n^{(K+1)} t^{K+1}| < 1$, we obtain approximately

$$\varepsilon_{nl}^K \sim \omega \left| \tau_n^{(K+1)} J_n^{(l+K+1,K)} \right|. \tag{27}$$

Note that if the frequency ω increases, the value of t must be reduced to provide a convergence of the series (22).

The error of Lth order amplitude approximation (23) for fixed K has the form

$$e_n^L = \left| I_n^{(L+1,K)} - I_n^{(L,K)} \right| = \left| \Phi_n^{(L+1)} J_n^{(L+1,K)} \right|. \tag{28}$$

As a result, for each n $(1 \leq n \leq N)$ the total error in the expansion (24) can be roughly estimated as

$$\varepsilon_n \leqslant (L+1)\varepsilon_n^K + e_n^L. \tag{29}$$

If the condition (29) is violated, then the series (22) or (23) converge slowly and the suitability of the approximation (24) is doubtful.

It follows that the overall error of eq. (18) satisfies the inequality

$$\varepsilon \leqslant N \max_{0 \leqslant n \leqslant N} \{\varepsilon_n\}. \tag{30}$$

In addition to the error of KH approximation (10), this error estimate can be used to formulate the validity conditions of the method.

3. Remarks on the Numerical Implementation

A C program was implemented to evaluate synthetic body wave seismograms for 2-D multilayered media. The medium can be composed of several isotropic or transversely isotropic (TI), elastic or weakly absorbing layers, separated by curved regular or irregular interfaces. Figure 1 depicts a principal flow chart of the numerical algorithm used. By analogy with the scalar case (DRUZHININ, 1994), it consists of two parts: (a) the computation of KH kernel (cf. eq. (10)) and (b) numerical integration according to eq. (18). Thereafter, an approximate inverse transform (15) is applied to obtain a final time-domain response.

The first step in our computations is the evaluation of boundary wave field given by eq. (2) (Fig. 1). Once the unknown boundary wave field is determined, the KH kernel can be calculated by substituting the boundary values into eq. (16). Moreover, the branch points in the first part of eq. (6) are memorized to calculate the head-wave arrivals uniformly over the offset (cf. Appendix A).

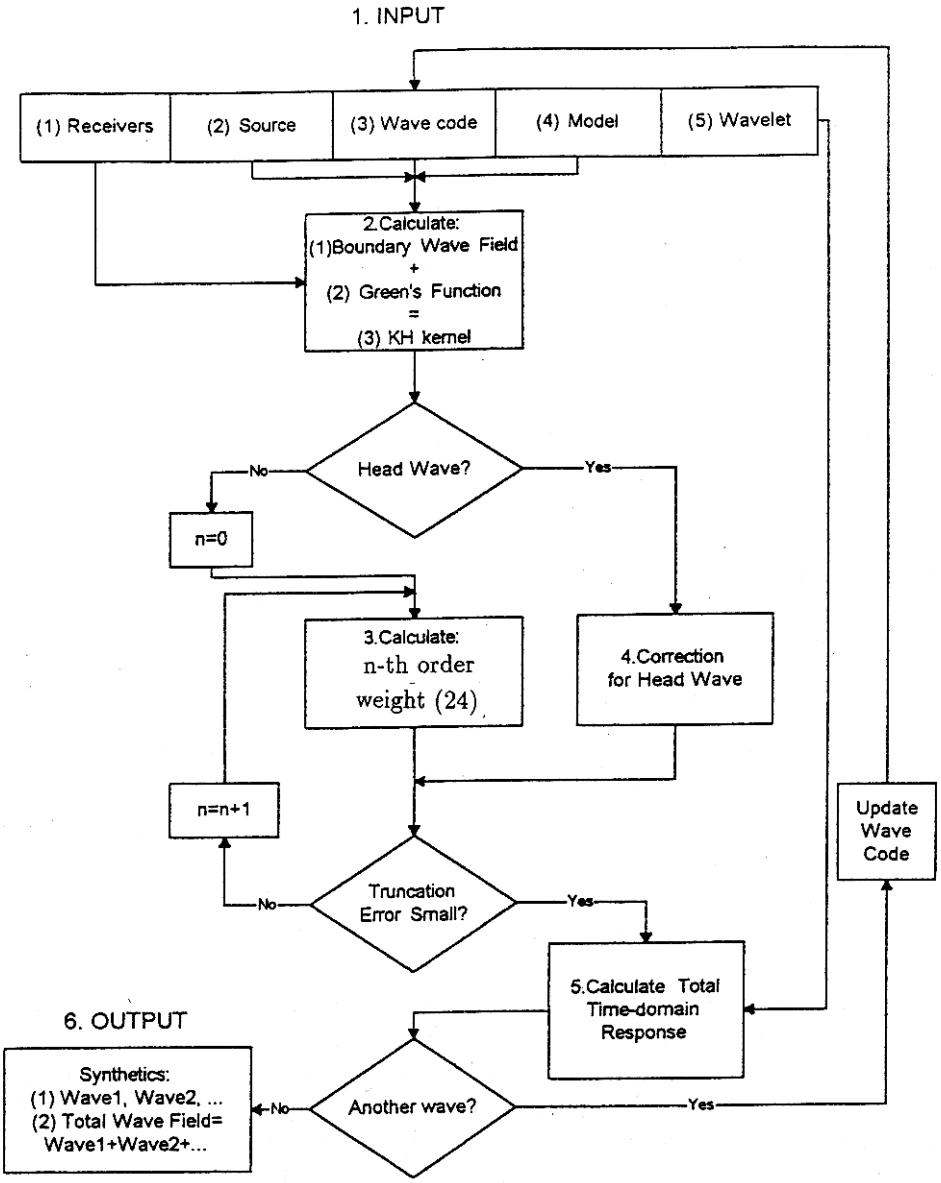

Figure 1
Principal flow chart of the KH numerical algorithm proposed.

Next, the components (8) are evaluated upon use of the well-known elementary source solutions whenever possible. In more complicated models, these components are expanded into the WKBJ series (SINGH and CHAPMAN, 1988; WENZEL *et al.*, 1990). By putting the source location $\mathbf{x}'$ into a complex space, we may also construct an analytical extension of the diverging wave propagating away from this source (FELSEN, 1984; WU, 1985).

In situations where the ray-Kirchhoff approximation (FRAZER and SEN, 1985) is valid and the above elementary and numerical solutions cannot be effectively used to handle the problem, standard ray-tracing procedures are applied to compute the amplitudes (16) and phase functions (17) of the secondary waves. They are needed to propagate ART data (without geometrical spreading) from the source to (usually) the last interface according to the specified ray code. If the boundary is well-defined at the ray intersection points (assumed for the time being to be off the critical angle region), we compute travel times and reflection/transmission coefficients for a corresponding outgoing wave. Equations (6) are then applied layer by layer to continue a wave field across each interface. We next compute the Green's function terms (11).

Our program deals with the numerical evaluation of the KH integral (10) by means of eq. (18) and makes use of the estimate of the truncation error (30). We have to evaluate the coefficients in the series (22) as well as eq. (25) to define the directivity pattern (21) and also to estimate the truncation error. Certainly, we start from the simple zero-order quadrature formula, which corresponds to the trapezoidal formulae for the oscillatory integrals (FRAZER, 1988; HAIGER and LIU, 1992). As indicated earlier, they have been considered before to compute the KH integral (WU, 1985; KOOPMAN *et al.*, 1989). If the overall error (30) is not small enough then we consider a higher-order special function (25). We continue this iterative process until the error is less than a specified tolerance level (Fig. 1). It is worth noting that, due to the fast convergence of the series (22) and (23), we have often obtained $L = 1$ and $K \leqslant 3$ (STAMNES *et al.*, 1983; DRUZHININ, 1994). Note, however, that, although there are higher-order corrections to the phase function (17), there are no higher-order corrections to the amplitude function (16) due to the high-frequency condition (12).

Finally, the total wave field is constructed as a superposition of all elementary body waves of interest specified by a given wave code such as reflected, refracted, converted, etc. (Fig. 1). This is similar to the superposition of the reflection operators by KENNETT (1984) (for more details, cf. DRUZHININ and KIM, 1995).

4. Comparison with Other Methods

Compared with other methods, the numerical algorithm discussed above offers the following advantages:

(1) unlike finite-difference or finite-element methods, it is not time-consuming and does not require much memory (for example, the total CPU time of the desk-top computer required to compute the synthetic examples presented in this paper was about 5 min.).

(2) it removes the disadvantages of the ART algorithms concerning singular regions of ray field (i.e., critical angles, caustics and diffractions).

(3) it can be effectively combined with other methods due to the fairly general representations (2), (6) and (8). Such hybrid representation makes it possible to avoid the difficulties associated with either of these methods by optimizing the advantages of each.

(4) the well-known limitations of the beam methods (BEN-MENAHEM and BEYDOUN, 1985) and related techniques (KLEM-MUSATOV and AIZENBERG, 1989; WANG and WALTHAM, 1995) are eliminated. Neither paraxial approximations (BEN-MENAHEM and BEYDOUN, 1985) nor additional diffracted ray tracing (HANYGA, 1993, 1995) or boundary-layer amplitude estimates (KLEM-MUSATOV and AIZENBERG, 1989) were involved (cf. Appendix B).

(5) the computation of the KH integral (10) is done directly without the case splitting analysis of ray singularity type in the vicinity of stationary points which is needed in asymptotic methods (HANYGA, 1993; KRAVTSOV and ORLOV, 1993).

(6) in the ray-Kirchhoff techniques (HADDON and BUCHEN, 1981; SCOTT and HELMBERGER, 1983; FRAZER and SEN, 1985; GELIUS, 1993; TYGEL *et al.*, 1994), it is assumed that the KH integrand (16) is regular throughout the integral surface. In the present algorithm, no assumptions of this sort must be made.

The weak points of the program are the following:

(1) the wave code is assumed to be the same for all rays spreading from the source. To consider composite regions of a general type, we must transform them to layered models by introducing artificial boundaries (ČERVENÝ *et al.*, 1977). This is often inconvenient for the user.

(2) in practice, it is rather difficult to compute multiple scattering effects if only the simple KH integral (10) is being considered.

(3) in some cases (e.g., grazing rays) the low-frequency background in eq. (9) cannot be dropped. The reason is that some additional interference waves generated by the source should be considered.

(4) in some models such as waveguides and at large epicentral distances, the total wave field may involve hundreds of elementary waves, rendering this program inefficient.

(5) if the boundary curvature gradient is too high compared with the wavelength, or the number of incoming waves is too large, eq. (6) in plane-wave approximation should be replaced by the T-matrix equations (BOSTRÖM, 1980).

(6) expressions have not yet been developed which unite the automatic computations of the high-order terms of eq. (24) with the Green's function computation in smoothly inhomogeneous layers of arbitrary variable velocity gradient.

5. Synthetic Examples

The synthetic examples presented in this section have been specially designed to demonstrate the usefulness of the algorithm discussed above. Features such as the accuracy and validity range of this algorithm are compared to those corresponding to the boundary element and other particular solutions of interest. For convenience, the only absolute value of vector wave field (10) is depicted throughout. Although the polarization and wave type conversion effects are simulated sufficiently, they are not subject to the present investigation.

5.1 *Test of Accuracy*

In order to check the accuracy and computational stability of the algorithm, we have calculated some well-known special functions of the diffraction theory which are also known from the singularity theory (HANYGA, 1993; KRAVTSOV and ORLOV, 1993). Similar numerical integrations of the classical diffraction integrals have been established by DRUZHININ (1994). Details may be found in DRUZHININ and KIM (1995).

When an A_3 singularity (i.e., cusp caustic) occurs, we evaluate the Pearcey's integral

$$Pe(x, y) = P(x, y) + P(x, -y),\ P(x, y) = \int_0^\infty \exp[i(u^4 + xu^2 + yu)]\, du.$$

Each term of this representation is computed in the range of arguments $2 \leqslant x \leqslant 8$, $0 \leqslant y \leqslant 8$ with grid interval $\Delta x = \Delta y = 2$. The parameters of the numerical expressions (eq. (18)) with weights (24) were $N = 10^2$, $L = 0$ and $K = 2$. A comparison with the error-predictive Gaussian quadrature formula (CONNOR and CURTIS, 1982) demonstrates the accuracy of such formula up to the 5th significant figure for all values of arguments x and y (cf. Table 1). Similar result has also been achieved for $N = 10^3$, $L = 0$ and $K = 1$.

5.2 Anisotropy

Let us consider the TI homogeneous space specified by the density-normalized elastic constants $C_{11} = 26.56$, $C_{33} = 10.97$, $C_{13} = 6.66$, $C_{44} = 1.87$, and $C_{66} = 7.23$ (km^2 s^{-2}) that would correspond to the stratified model 'Plex-Alum' from WHITE (1982). The receivers are located on the circle of radius $R = 1$ km with center at the source point. They are specified by the above polar angle θ measured from the anisotropy axis z. The integration contour represents a circle of radius $R/2$. It consists of 10^3 grid points distributed within a segtment $-40° \leqslant \theta \leqslant 130°$. A 20 Hz narrow-band Ricker's signal is used as the input wavelet. A plane-wave formulation of eq. (10) (WENZEL *et al.*, 1990) leads to the WKBJ technique (SINGH and

Table 1

Real (I) and imaginary (II) parts of the Pearcy's integral Pe(x, y) calculated by numerical formula (18) (A) and their tabular values from CONNOR *and* CURTIS *(1982) (B).*

		I	I	II	II
x	y	A	B	A	B
2	0	0.924029	0.92403	0.729007	0.72901
4	0	0.646979	0.64698	0.593695	0.59370
6	0	0.520848	0.52085	0.500054	0.50005
8	0	0.447915	0.44792	0.437618	0.43762
2	2	0.993721	0.99372	0.312731	0.31273
4	2	0.740098	0.74010	0.413323	0.41332
6	2	0.587735	0.58773	0.403529	0.40353
8	2	0.495820	0.49582	0.376681	0.37668
2	4	0.596479	0.59648	−0.565160	−0.56516
4	4	0.766598	0.76660	−0.132658	−0.13266
6	4	0.683906	0.68391	0.081293	0.08129
8	4	0.588823	0.58882	0.169333	0.16933
2	6	−0.476832	−0.47683	−0.509207	−0.50921
4	6	0.225514	0.22551	−0.668159	−0.66816
6	6	0.515897	0.51590	−0.405727	−0.40573
8	6	0.565948	0.56595	−0.192537	−0.19254
2	8	−0.308926	−0.30892	0.545153	0.54515
4	8	−0.567033	−0.56703	−0.308136	−0.30814
6	8	−0.096571	−0.09657	−0.614553	−0.61455
8	8	0.229865	0.22986	−0.532415	−0.53241

CHAPMAN, 1988) which was applied to simulate the qP and qSV wave propagation due to a point source in such model. The results in Figures 2 and 3 do not contain the source directivity function. Moreover, the synthetic seismograms contain only the main component of the wave polarization, representing a scalar product of the displacement vector with the corresponding unit polarization vector. Figure 2a demonstrates the WKBJ and the far-field solution by BEN-MENAHEM and SENA (1990). The discrepancy, which increases slightly in the neighborhood of the x axis, is due to the well-known limitation of the far-field solution in the domains of high wave-front curvature (BEN-MENAHEM and BEYDOUN, 1985; FRADKIN, 1989). In general, both methods are in satisfactory agreement with each other. The quasi-shear wave loop travel-time curve and the corresponding synthetic seismogram are shown in Figure 3. We can observe the regular behavior of the wave field near the cusps as well as the diffracted arrivals in the caustic shadow zone ($\theta < 20°$ and $\theta > 70°$) that cannot be predicted by the standard ART. Note that it is possible to visualize the effect of interference of the two wave forms (e.g., the 60-degree arrival at 0.45 s in Fig. 3b). This example shows that the WKBJ technique can simulate the Green's function in anisotropic media.

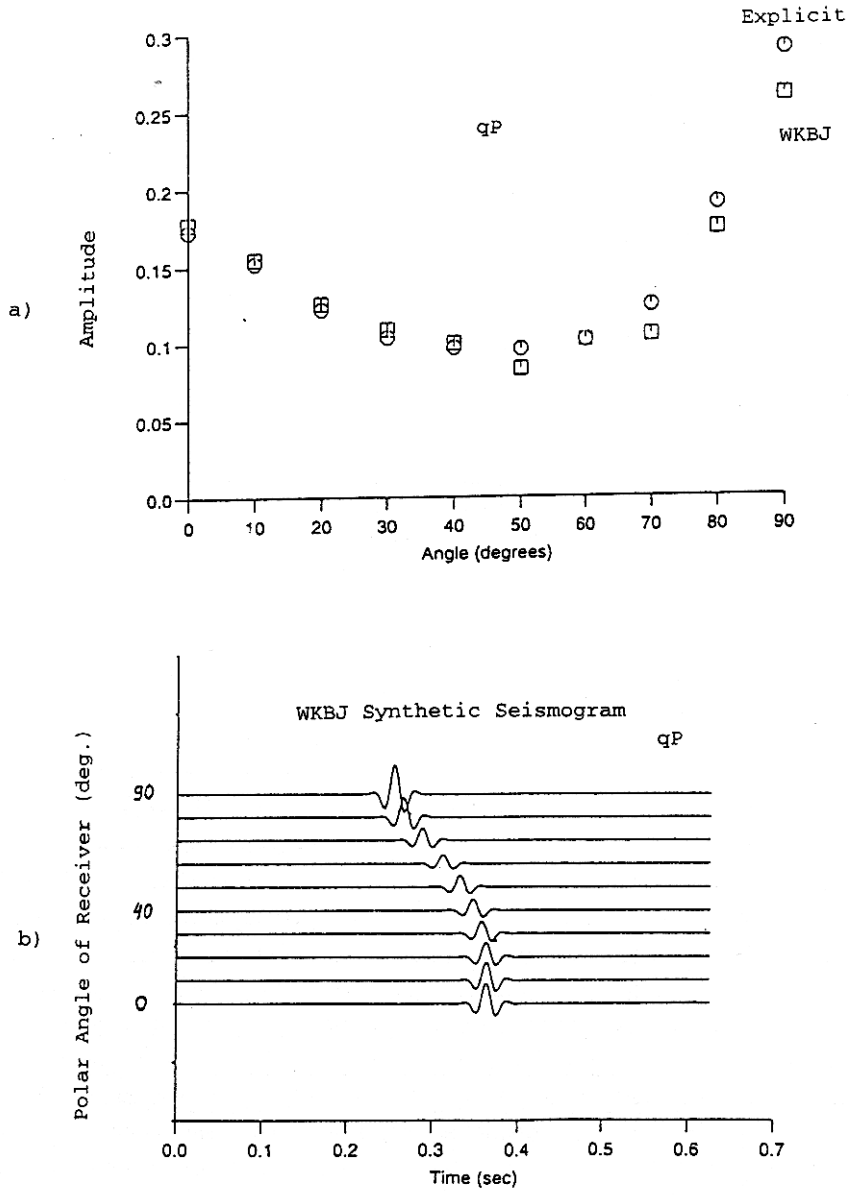

Figure 2
Amplitude of the qP wave with unit source directivity pattern in the 'Plex-Alum' model (WHITE, 1982) evaluated by the WKBJ technique (squares) and compared with the far-field approximation by BEN-MENAHEM and SENA (1990) (circles) (a). The former was used to compute the product of the qP wave field and the corresponding polarization vector (b).

a)

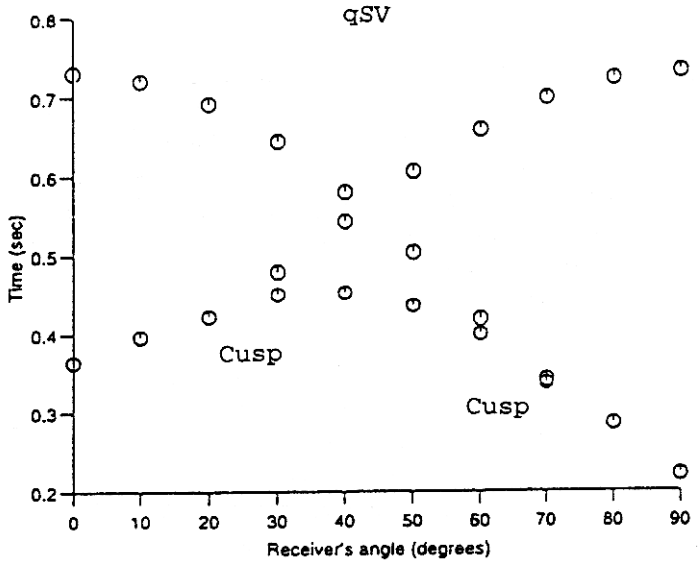

b)

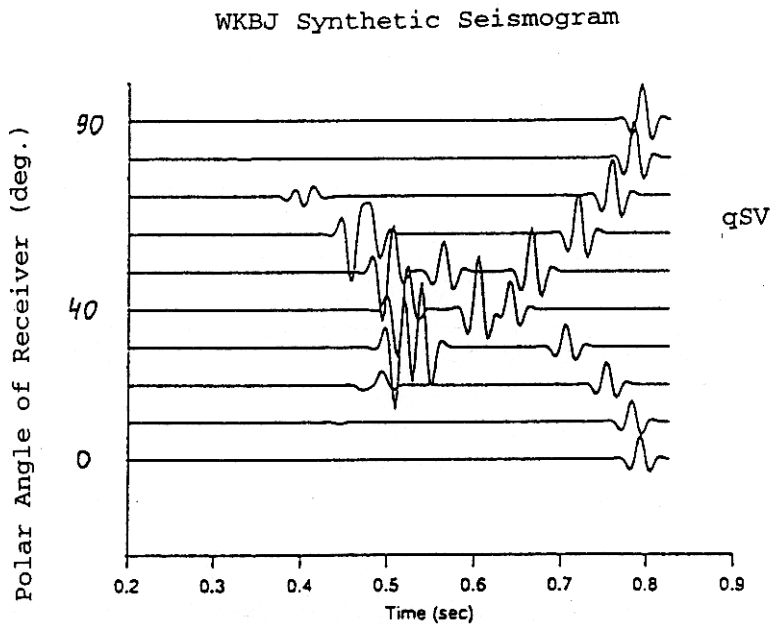

Figure 3

Travel-time plot (a) and synthetic seismogram (b) of the qSV wave with unit source directivity pattern in the 'Plex-Alum' model (WHITE, 1982) as evaluated by the WKBJ technique. The seismogram represents the product of the time-domain qSV vector wave field and the corresponding polarization vector. The travel-time curve was constructed by picking the first arrivals in Figure 3b.

5.3 Reflection Problem

Next, we compute the PP wave field reflected from the curved interface between two homogeneous isotropic media specified by the following elastic parameters: $v_{p1} = 4$ km/s, $v_{s1} = 2.3$ km/s, $\rho_1 = 2.5$ g/cm^3 (top layer) and $v_{p2} = 6$ km/s, $v_{s2} = 3.46$ km/s, $\rho_2 = 2.7$ g/cm^3 (bottom half-space). The triplicated travel-time curve and the corresponding ray diagram with a simple caustic can be viewed in Figure 4. The source is located at (0, 0.2) (km) and the receivers are distributed along the horizontal line $z = 0$ within the interval $0 \leq x \leq 7$ (km).

Figure 5a is the 2 Hz amplitude versus offset in the caustic shadow, evaluated using eq. (18) (solid line) and the Indirect Boundary Element Method (IBEM, dashed line). The IBEM results were obtained by adapting the formulation of SÁNCHEZ-SESMA and CAMPILLO (1991) and PEDERSEN *et al.* (1996) to an explosion in the model geometry shown in Figure 4b. In Figure 5b, we compare the zero-offset 2 Hz wave forms computed by these two methods and by the WKBJ technique used in the previous example (see also WENZEL *et al.*, 1990). It is apparent from Figure 4, that the performance of KH is satisfying near the caustic where the ART is not valid. The amplitude error of the KH method in the deep shadow zone ($x > 6$ km, Fig. 4a) is probably due to neglection of the low-frequency term in eq. (9). Numerical tests by DRUZHININ and CAMPILLO (1996) demonstrate that the discrepancy between the KH and IBEM wave forms in Figure 4b is due to the error of the time-domain eq. (15). Such tests also reveal a significant error of the WKBJ wave forms in the domains of the large reflector's curvature in the wavelength scale.

Reflected PP waves were computed for different models of the top layer in Figure 4b. Figure 6 shows the KH synthetic seismograms evaluated for a) constant P velocity of 4 km/s, b) constant vertical velocity gradient $v(z) = 4 + 0.1z$ km/s and d) similar velocity law, but with nonvertical (45°) velocity gradient, e) weak anisotropy with the anisotropy coefficient $\eta = 0.95$ in notations by BEN-MENAHEM and SENA (1990), and f) slightly absorbing medium with the frequency-independent* exponential decay factor $\exp(-\gamma r)$ where $\gamma = 0.1$[1/km] and r is distance in km. We have attempted to demonstrate the effect of above elastic properties on the wave field. One can also compare the results in Figure 6b with the diffracted wave field produced by the broken interface (Fig. 7a) in the same direction (cf. Fig. 6c). Note that the earlier linear arrivals in Figure 6 correspond to the reflections from lateral parts of the interface ($|x| > 1$).

The example in Figure 7 continues the analysis concerning diffracted waves generated by the irregular interface. In Figure 7a, the interface offset is 0.1 km for $-0.5 < x < 0.5$ km and 0.15 km for another two interface offsets. Note that the normal diffracted events can be observed in Figure 7d. In the asymptotic theory

* Because of the narrow-band wavelet being used.

a)

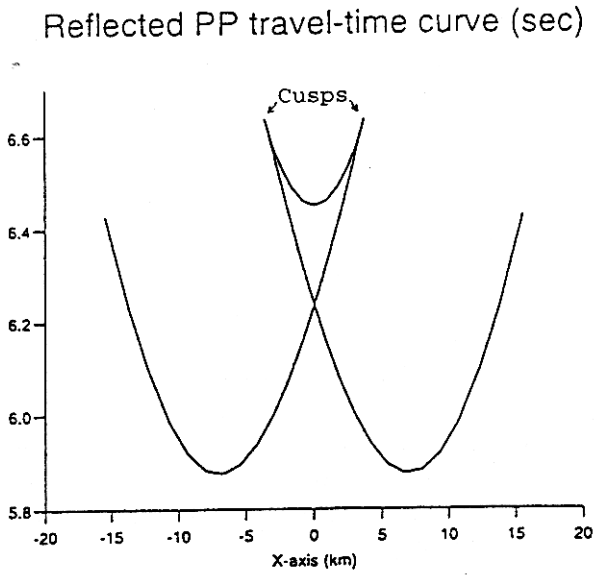

b)

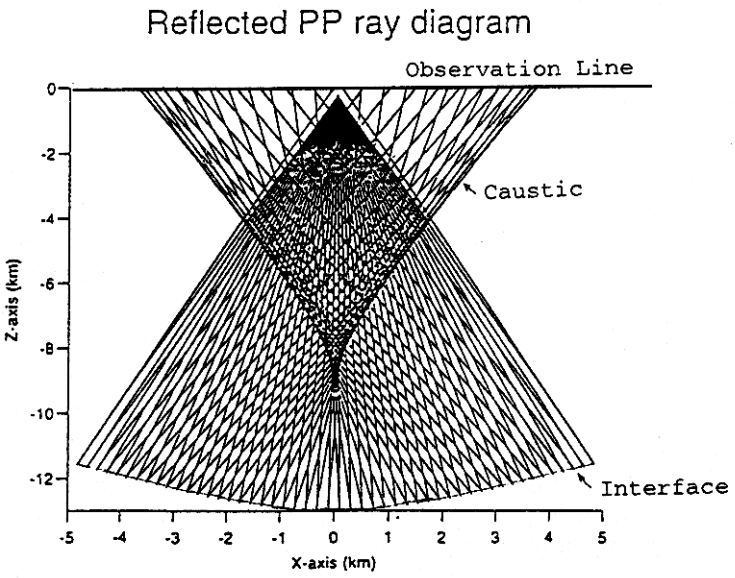

Figure 4

Travel-time plot (a) and ray diagram (b) of the reflected PP wave in two-layered homogeneous isotropic model with a smooth curved interface. The P velocities are 4 and 6 km/s for the top and bottom layers, respectively. Note that the horizontal and vertical scales are different.

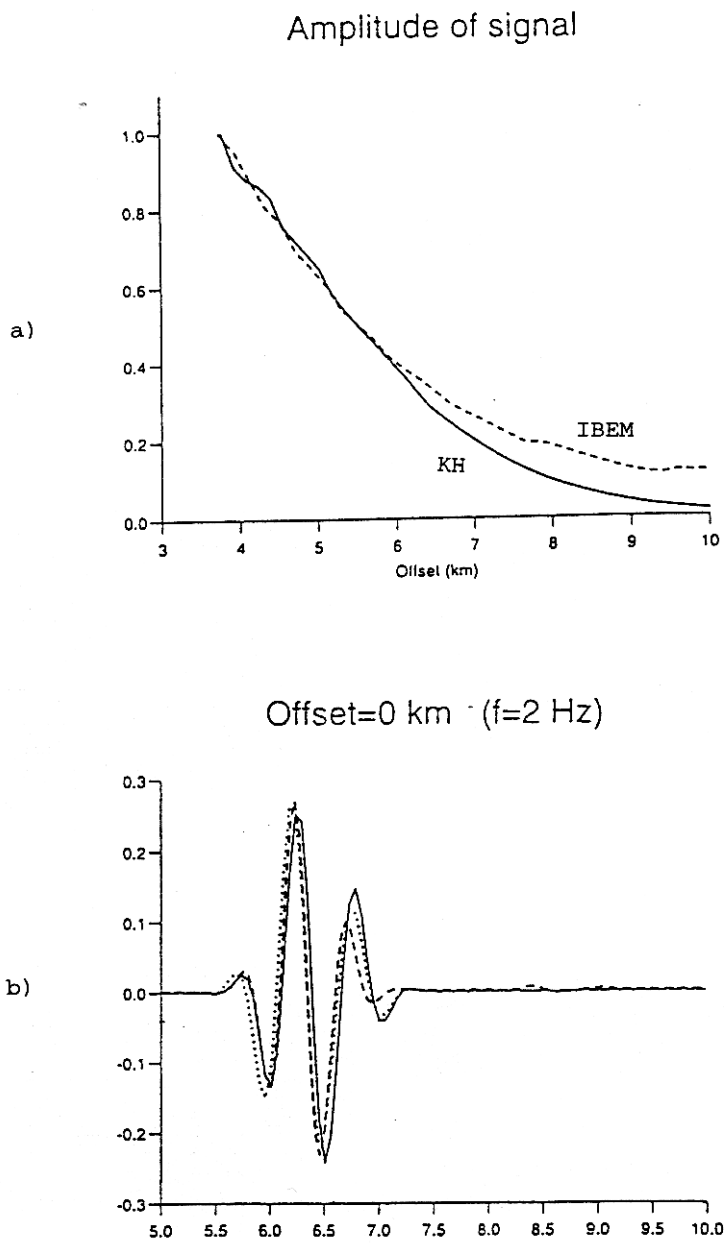

Figure 5
Low-frequency (2 Hz) amplitude versus offset (a) and the zero-offset waveform (b) near the caustic of reflected rays shown in Figure 4b. The absolute value of the reflected PP wave field was evaluated upon use of the WKBJ technique (dots), the present algorithm (solid line), and the IBEM (dashed line).

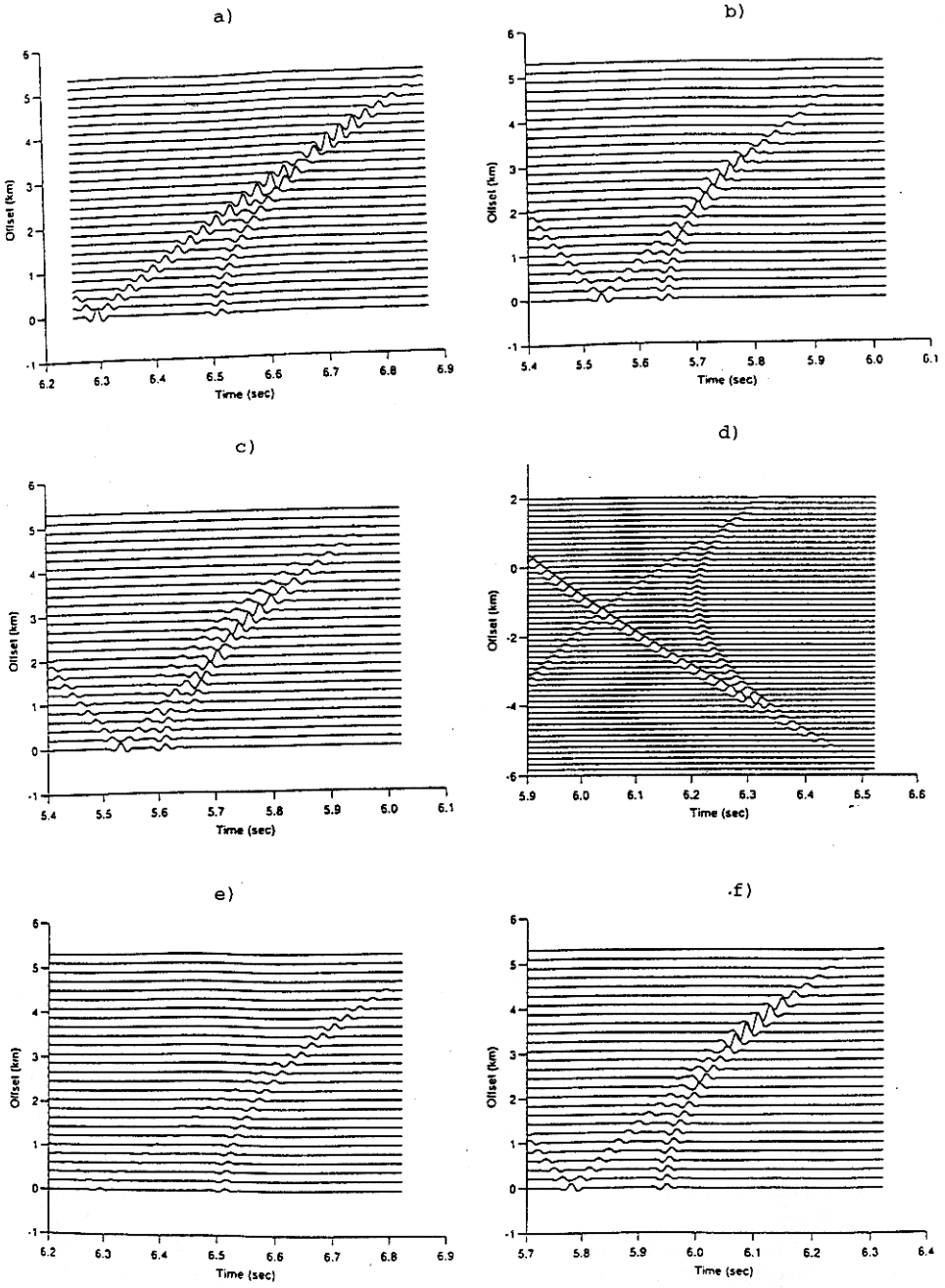

Figure 6

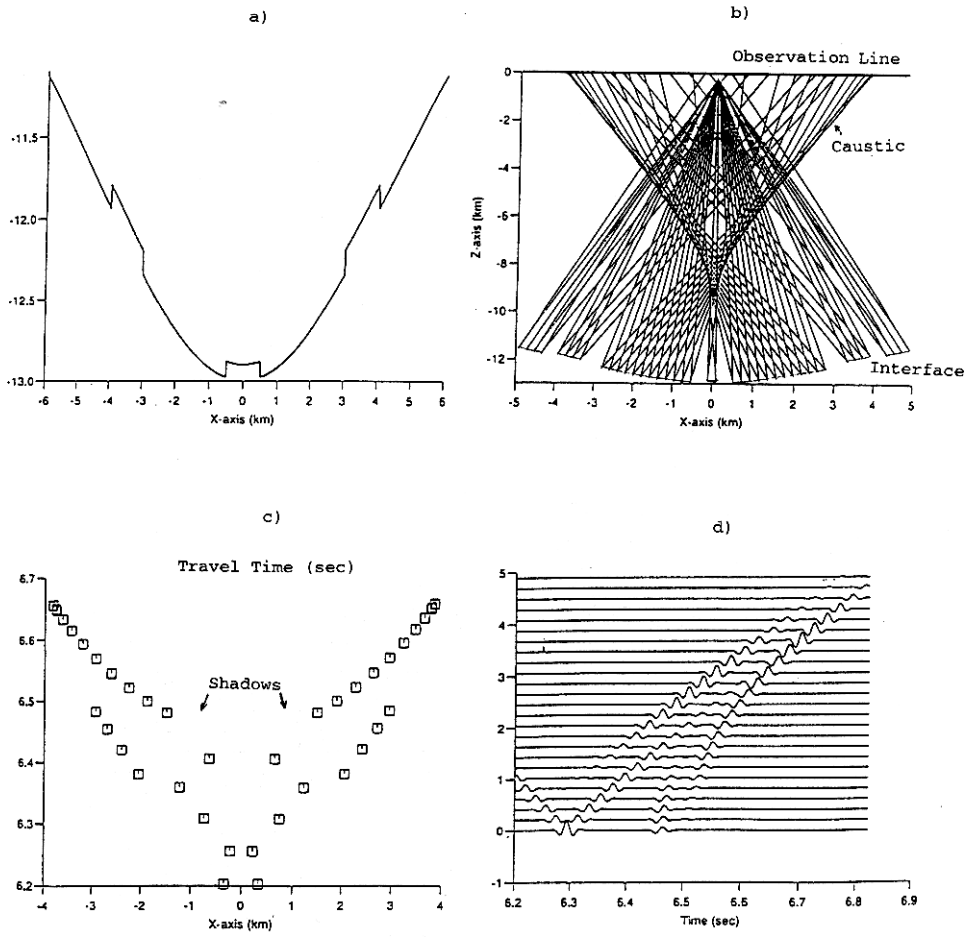

Figure 7

Geometry of the irregular interface (a), ray diagram (b), travel-time plot (c), and KH synthetic seismogram (d) of the reflected PP wave. P velocities are of 4 and 6 km/s for the top and bottom layers, respectively. The input wavelet is a 20 Hz narrow-band Ricker's signal. The seismogram represents a product of the time-domain qP vector wave field and the corresponding polarization vector. Note that the horizontal and vertical scales are different.

Figure 6

KH synthetic seismograms of the reflected PP waves for different models of the top layer in Figure 4b: a) constant P velocity of 4 km/s, b) constant vertical velocity gradient $v(z) = 4 + 0.1z$ km/s, d) similar velocity law, but with tilted (45°) velocity gradient, e) weak anisotropy with the anisotropy coefficient $\eta = 0.95$ in notations by BEN-MENAHEM and SENA (1990), and f) slightly absorbing medium with the exponential decay factor $\exp(-\gamma r)$ where $\gamma = 0.1/\omega$ and r is distance. Synthetic seismogram in Figure 6c was constructed for the constant vertical velocity gradient $v(z) = 4 + 0.1z$ km/s of the top layer and the irregular interface shown in Figure 7a. The input wavelet is a 20 Hz narrow-band Ricker's signal. The seismogram represents a product of the time-domain qP vector wave field and the corresponding polarization vector.

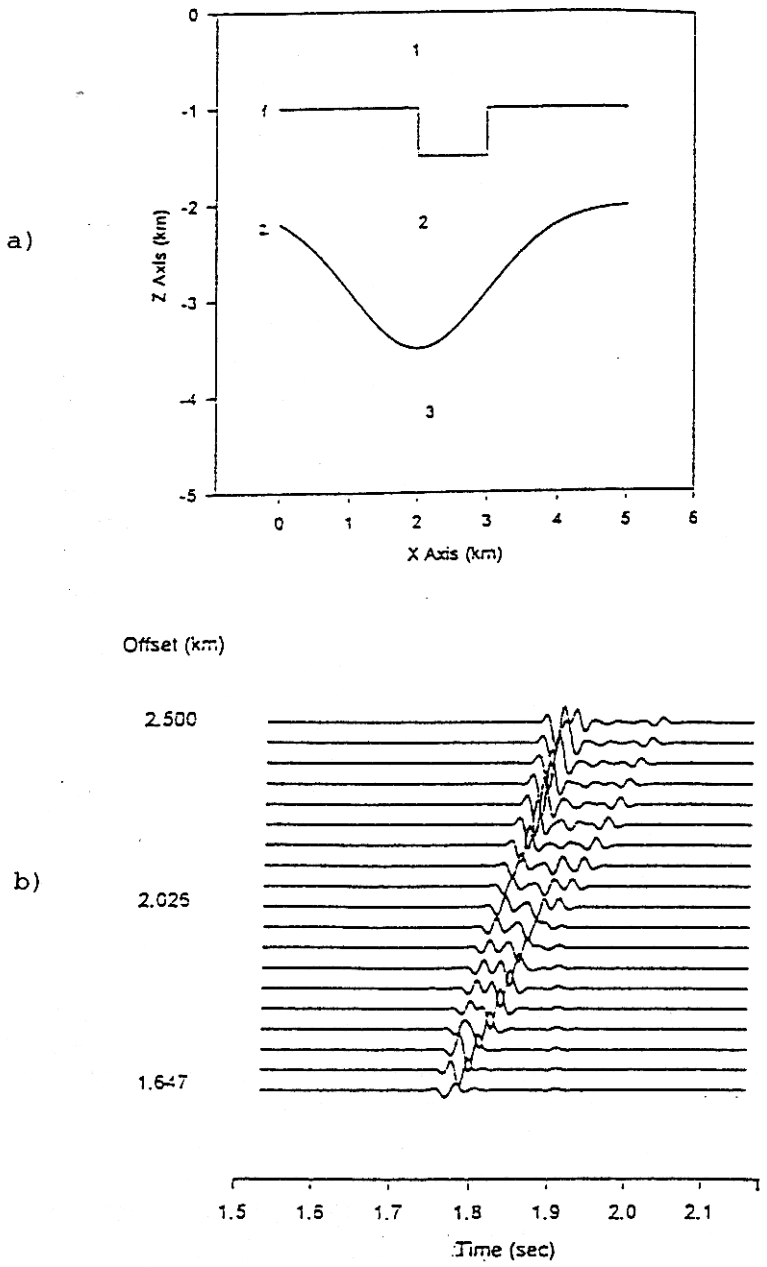

Figure 8
Geometry of the three-layered TI model from DRUZHININ and KIM (1995) (a) and the KH synthetic seismogram of transmitted primary P3P2P1 wave field of frequency 20 Hz (b). The seismogram represents a product of the time-domain qP vector wave field and the corresponding polarization vector.

(KRAVTSOV and OPLOV, 1993; HANYGA, 1993), such events correspond to the so-called edge catastrophes described in terms of the incomplete Airy functions and their extensions. In this example, eq. (10) was integrated directly without the case splitting analysis of broken caustics near the corresponding shadow boundaries shown in Figures 7b, c (for a more detailed discussion, cf. Appendix B).

5.4 Transmitted Waves

In Figure 8a, we show a three-layered TI model with irregular (top) and curved (bottom) interfaces from DRUZHININ and KIM (1995). The elastic parameters of the layer 2 correspond to the model 'Plex-Alum' (WHITE, 1982) and those of layer 3 to the real weakly anisotropic rock sample 'Timber Mountain tuff' (BEN-MENAHEM and SENA, 1990), respectively. Five density-normalized elastic parameters of the layer 1 are the following: $C_{11} = 10.0$, $C_{33} = 6.4$, $C_{13} = 2.3$, $C_{44} = 5.3$, and $C_{66} = 3.6$ (km^2 s^{-2}). A primary P3P2P1 transmitted wave is generated by the point source 'explosion' located at (2, -6) (km) (layer 3) and observed at the earth's surface $z = 0$. The surface Σ coincides with the top (irregular) interface depicted in Figure 8a. The KH seismogram can be seen in Figure 8b. It shows the waves which are transmitted via the plane segments of Σ including the subvertical segment along the vertical line $x = 2$ km; their rays contain few shadows due to the presence of sharp edges with corresponding edge effects. Also, Stoneley wave propagating along the step discontinuity of Σ appears at 1.9 sec. A seismogram of the converted P3S2S1 wave with a triplicated wave front in the vicinity of the z axis due to the anisotropy of layer 1 was computed by DRUZHININ and KIM (1995) (p. 159).

These results confirm that the present approach can successfully compute synthetic seismograms for more or less realistic structures.

6. Discussion and Conclusions

The principal goal of this paper was to set up a general KH equation for the diffraction/scattering of elastic waves under a variety of boundary conditions, in a form most suited to efficient numerical computation.

We have restricted ourselves to the high-frequency case to express the KH kernel in the most convenient form for carrying out the numerical quadratures. However, eq. (10) does not imply that the kernel is computed in the ART approximation.

A number of assumptions such as (12)–(14) must apply for eq. (18) to be valid. Nevertheless, it is clear that a very wide class of problems of the kind illustrated in our synthetic examples fulfill these conditions in contrast to the validity conditions of the ART and its modifications (ČERVENÝ *et al.*, 1977; BEN-MENAHEM and BEYDOUN, 1985; FRADKIN, 1989).

It may appear as if we have actually complicated the solution of the problem by introducing the fairly general representations. However, the above procedure seems to be necessary if we want to extract the KH theory for a general case. Hence, our results extend the existing ray-Kirchhoff methods.

Their usefulness is restricted only to the classes of media for which the Green's tensor is known. We have used a more or less generic representation (7) that provides the necessary degrees of freedom.

In order to illustrate additional properties of the formalism, we also consider a head-wave contribution of the branch points (cf. Appendix A) and the problem of numerical Green's function computations by means of the WKBJ technique (after WENZEL *et al.*, 1990).

According to FRAZER and SEN (1985), the main limitation of eq. (10) is that an outgoing wave is assumed to have interacted only once with the boundary representing the integral surface. Consequently, one question remaining is to remove this limitation. In this regard, a combination of our results with the T-matrix approach (e.g., BOSTRÖM, 1980) should be useful.

To obtain numerical results we consider the truncated solutions. A closer study of the convergence properties of these truncated solutions is of primary interest. In this regard, the choice of the proper segment size is a very important factor in any KH formulation under condition (12). We found that the results become accurate when the phase and amplitude polynomial expansions (22) and (23) are used to engender a family of well-known special functions (25). In some examples even the zero-order terms of these expansions produced the results in satisfactory computation precision. Nevertheless, we need the higher order terms to compute the overall truncation error (30). As a result, the final numerical algorithm has a self-predictive truncation error.

We employed numerical tests to discuss the accuracy and validity of the method by comparing it to other methods. Numerical results for different models show the high performance of our method.

Acknowledgements

This research has been sponsored in part by the International Science Foundation under grant Nos. RPH000 and RPH300, by the Russian Foundation of Basic Research under grant No. 94-05-16533, by the NATO Scientific and Environmental Affairs Division under grant No. ENVIR.CRG 940971, and by the Basic Science Research Institute Program, Ministry of Education of S. Korea, 1995, Project No. BSRI-94-5402. Our special thanks are due to Dr. T. Taner for the financial support. We are greatly indebted to L. Klimeš, W. B. Beydoun, A. Hanyga and I. Pšenčik for their critical comments which improved the clarity of this paper. Useful discussions with S. Goldin, O. Coutant, M. Bouchon, F. J. Sánchez-Sesma, S. Gaffet,

J. Virieux, J. Pajchel, D. Lokshtanov, and R. O'Doherty are greatly appreciated. The paper has been originally submitted to the topical issue of Pure and Applied Geophysics 'Seismic Waves in Laterally Inhomogeneous Media', eds. I. Pšenčík, V. Červený, L. Klimeš. The authors are grateful to the editors for their editorial assistance.

Appendix A: Corrections for Head Waves

Let us suppose that the reflection coefficient $K(s)$ from eq. (6) as a function of the arclength s has a branch point $\mathbf{x}'_b$ specified by some value $s = s_b$. This coefficient can now be written (BREKHOVSKICH, 1980)

$$K(s) = \sum_{a=1}^{2} K_a(s) h_a(s)$$

where

$$h_a(s) = \begin{cases} 1 & a = 1 \\ \sqrt{s - s_b} & a = 2 \end{cases} \quad \text{for} \quad \text{and} \quad K_a(s)$$

are regular functions in the vicinity of $\mathbf{x}'_b$. Then, eq. (18) takes the following form

$$u(\mathbf{x}) = \sum_{a=1}^{2} u_a(\mathbf{x})$$

with two terms

$$u_a(\mathbf{x}) = \sum_{n=1}^{N} \Delta u_a(\mathbf{x}, \mathbf{x}'_n)$$

in which

$$\Delta u_a(\mathbf{x}, \mathbf{x}'_n) = \Delta u_a^{(0)}(\mathbf{x}, \mathbf{x}'_n) \Delta I_{na},$$

$$\Delta I_{na} = \frac{1}{\Delta s_n} \int_{\Delta \Sigma_n} \Delta u_{na}(\mathbf{x}, \mathbf{x}')\, ds'.$$

To define the solutions $\Delta u_a^{(0)}$ and Δu_{na} instead of $\Delta u^{(0)}$ and Δu_n given in eqs. (20–21), the coefficient K is simply replaced by K_2. In the equations above, the first term represents the ordinary reflected wave field, whereas the second term is governing the head-wave arrivals associated with the critical ray at $\mathbf{x}'_b$.

The phase and amplitude expansions (22) and (23) in the second term yield a result similar to eq. (24)

$$\Delta I_{n2} \sim I_{n2}^{(L,K)} = \sum_{l=0}^{L} \Phi_{n2}^{(l)} J_{n2}^{(l,K)},$$

$$J_{n2}^{(l,K)} = \int_{x-}^{x+} t^l h_2(t) \exp\left(i\omega \sum_{k=1}^{K} \tau_n^{(k)} t^k \right) dt$$

where $h_2(t) = \sqrt{t - t_b}$, $t_b = (s_b - s_n^0)/\Delta s_n$, $\Phi_{n2}^{(l)}$ are the coefficients of the amplitude expansion after the replacement of K by K_2. Thus, we derive a new family of special functions. In practice, we usually need only the special function for $K = 2$ that can be transformed into the well-known parabolic cylinder function D_l (BREKHOVSKICH, 1980). This result is similar to the expressions for head waves obtained by ART at large distances beyond the critical angle point (ČERVENÝ and RAVINDRA, 1971). Numerical examples can be found in DRUZHININ and KIM (1995) (pp. 161–162).

Appendix B: Scalar Diffraction Modelling

Let a wave field be represented by scalar P or SH velocity potential. Consider the irregular interface Σ in Figure 6. According to step 2 in Figure 1, the Green's function $g(\mathbf{x}'', \mathbf{x}')$ was computed in each point $\mathbf{x}' \in \Sigma$ for $\mathbf{x}'' = \mathbf{x}_s$ (source) and $\mathbf{x}'' = \mathbf{x}$ (receiver) by use of the well-known explicit formulae (BEN-MENAHEM, 1990). In this specific case, the usual ART approximation (FRAZER and SEN, 1985; TYGEL *et al.*, 1994) was applied to compute the reflected wave field at Σ (see eq. (2) for $P = 1$). It is expressed in terms of the Green's function $g(\mathbf{x}_s, \mathbf{x}')$ and the plane-wave reflection coefficient K from eq. (6). We construct the amplitude and phase functions of the scalar KH integrand

$$U(\mathbf{x}_s, \mathbf{x}', \mathbf{x}) = i\omega K U(\mathbf{x}_s, \mathbf{x}') U(\mathbf{x}', \mathbf{x}) \phi(\mathbf{x}_s, \mathbf{x}', \mathbf{x})$$

and

$$\tau(\mathbf{x}_s, \mathbf{x}', \mathbf{x}) = \tau(\mathbf{x}_s, \mathbf{x}') + \tau(\mathbf{x}', \mathbf{x}),$$

where $\phi(\mathbf{x}_s, \mathbf{x}', \mathbf{x}) = \mathbf{n}' \cdot [\mathbf{p}^+(\mathbf{x}_s, \mathbf{x}') - \mathbf{p}(\mathbf{x}, \mathbf{x}')]$, $\mathbf{p}^+(\mathbf{x}_s, \mathbf{x}') = \nabla' \tau(\mathbf{x}_s, \mathbf{x}')$ is the slowness vector of the reflected wave (cf. eq. (6)) and $\mathbf{p}(\mathbf{x}, \mathbf{x}') = \nabla' \tau(\mathbf{x}, \mathbf{x}')$ is the slowness vector of the phase surface $\tau(\mathbf{x}, \mathbf{x}') = \text{const}$ at $\mathbf{x}'$, $U(\mathbf{x}'', \mathbf{x}')$ and $\tau(\mathbf{x}'', \mathbf{x}')$ are the amplitude and phase functions of the Green's function $g(\mathbf{x}'', \mathbf{x}')$. After the computation of appropriate quadrature weights (21) with automatic integration in eq. (24) (cf. step 3 in Fig. 1), the resulting time-domain response is (cf. eq. (15))

$$u(\mathbf{x}_s, \mathbf{x}; t) \sim Re \sum_{n=1}^{N} \Delta I_n U(\mathbf{x}_s, \mathbf{x}_n', \mathbf{x}; \omega') \Delta s_n f_s[t - \tau(\mathbf{x}_s, \mathbf{x}', \mathbf{x})].$$

Simple examples of such numerical formulae can be found in many papers (e.g., SCOTT and HELMBERGER, 1983; WU, 1985; KOOPMAN *et al.*, 1989). The same considerations apply to transmitted waves (HADDON and BUCHEN, 1981). The essential point here is that this formula simultaneously produces both reflected/transmitted waves and all diffractions. Instead of asymptotic techniques (KLEM-MUSATOV and AIZENBERG, 1989; WANG and WALTHAM, 1995; HANYGA, 1995), it leads to a computationally more efficient and less restrictive algorithm which does not require any information about the diffracted wave such as diffracted travel

time, diffraction coefficient, etc. Particularly, it removes the validity conditions of the paraxial or boundary-layer approximations (BEN-MENAHEM and BEYDOUN, 1985; KLEM-MUSATOV and AIZENBERG, 1989).

REFERENCES

BEN-MENAHEM, A., and BEYDOUN, W. B. (1985), *Range of Validity of Seismic Ray and Beam Methods in General Inhomogeneous media—I. General Theory*, Geophys. J. R. Astr. Soc. *82*, 207–234.

BEN-MENAHEM, A. (1990), *SH Waves from Point Sources in Anisotropic Inhomogeneous Media*, Geophysics *55* (4), 488–491.

BEN-MENAHEM, A., and SENA, A. G. (1990), *Seismic Source Theory in Stratified Anisotropic Media*, J. Geophys. Res. *95* (B10), 15395–15427.

BOSTRÖM, A. (1980), *Multiple Scattering of Elastic Waves by Bounded Obstacles*, J. Acoust. Soc. Am. *67* (2), 399–413.

BREKHOVSKICH, L. M., *Waves in Layered Media* (Academic Press, New York 1980).

ČERVENÝ, V., and RAVINDRA, R., *Theory of Seismic Head Waves* (University of Toronto Press, Toronto and Buffalo 1971).

ČERVENÝ, V., MOLOTKOV, I. A., and PŠENČIK, I., *Ray Method in Seismology* (Univerzita Karlova, Praha 1977).

CONNOR, J. N. L., and CURTIS, P. R. (1982), *A Method for the Numerical Evaluation of the Oscillatory Integrals Associated with the Cuspoid Catastrophes: Application to Pearcey's Integral and its Derivatives*, J. Phys. A. *15*, 1179–1190.

DONG, W., and SCHMITT, D. P. (1994), *Simplified Dynamic and Static Green's Functions in Transversely Isotropic Media*, Geophys. J. Int. *119*, 231–242.

DRUZHININ, A. B. (1993), *Attenuation of Seismic Waves in General Viscoelastic Media*, Russian Geology and Geophysics *34*, (9), 73–82.

DRUZHININ, A. B., and LUNEVA, M. N. (1993), *Seismic Waves in Layered Anisotropic Media with Slip Contact*, Pacific Ocean Geology *2*, 141–152 (in Russian).

DRUZHININ, A. B. (1994), *Seismic Modelling by Scalar Wave Beam Method*, Russian Geology and Geophysics *35* (5), 72–90.

DRUZHININ, A. B., and KIM, W., *Seismic Modeling and Travel-time Inversion in 2-D Inhomogeneous and Anisotropic Media* (Res. Rep. BSRI-95-5402, Gyeongsang National University, Chinju 1995).

DRUZHININ, A. B., and CAMPILLO, M., *Hybrid Seismic Modeling in Acoustic, Elastic, Anelastic, Inhomogeneous, and Anisotropic Media* (Res. Rep. ENVIR.CRG 940971, University Joseph Fourier, Grenoble 1996).

FELSEN, L. B. (1984), *Geometrical Theory of Diffraction, Evanescent Waves, Complex Rays and Gaussian Beams*, Geophys. J. R. Astr. Soc. *79*, 77–88.

FOREMAN, T. L. (1989), *An Exact Ray Theoretical Formulation of the Helmholtz Equation*, J. Acoust. Soc. Am. *86* (1), 234–246.

FRADKIN, L. JU. (1989), *Limits of Vaildity of Geometrical Optics in Weakly Irregular Media*, J. Opt. Soc. Am. A *6*, 1315–1319.

FRAZER, L. N., *Quadrature of wavenumber integrals*, In *Seismological Algorithms: Computational Methods and Computer Programs* (ed. Doornbos, D. J.) (Academic Press, New York 1988) pp. 279–288.

FRAZER, L. N., and SEN, M. K. (1985), *Kirchhoff-Helmholtz Reflection Seismograms in a Laterally Inhomogeneous Multi-Layered Elastic Medium—I. Theory*, Geophys. J. R. Astr. Soc. *80*, 121–147.

GELIUS, L-J., *Asymptotic Diffraction Theory with Applications in Tomography* (Ph.D. Thesis, The Norwegian Institute of Technology, Trondheim 1993).

HADDON, R. A. W., and BUCHEN, P. W. (1982), *Use of Kirchhoff's Formula for Body Wave Calculations in the Earth*, Geophys. J. R. Astr. Soc. *67*, 587–598.

HAIGER, Q., and LIU, L. C. (1992), *Fourier or Bessel Transformations of Highly Oscillatory Functions*, J. Phys. A. *25*, 6755–6760.

HANYGA, A., *Numerical Application of asymptotic diffraction theory*. In *Mathematical and Numerical Aspects of Wave Propagation* (Kleinman, R. *et al.*, eds.) (SIAM, Philadelphia 1993) pp. 246–258.

HANYGA, A. (1995), *Asymptotic Edge-and-vertex Diffraction Theory*, Geophys. J. Int. *123*, 277–290.

KENNETT, B. L. N. (1984), *Reflection Operator Methods for Elastic Waves. II Composite Regions and Source Problems*, Wave Motion *6*, 419–429.

KLEM-MUSATOV, K. D., and AIZENBERG, A. M. (1989), *The Edge Wave Superposition Method (2-D Scalar Problem)*, Geophys. J. Int. *99*, 351–367.

KOOPMAN, G. H., SONG, L., and FAHNLINE, J. B. (1989), *A Method for Computing Acoustic Fields Based on the Principle of Wave Superposition*, J. Acoust. Soc. Am. *86* (6), 2433–2438.

KRAVTSOV, Yu. A., and ORLOV, Yu.I., *Caustics, Catastrophes and Wave Fields* (Springer-Verlag, Berlin 1993).

LUMLEY, D., and BEYDOUN, W. (1993), *Angle-dependent Reflectivity Estimation by Kirchhoff Migration/ Inversion: Theory*, SEP Report No. *79*, pp. 205–225.

PAO, Y-H., and VARATHARAJULU, V. (1976), *Huygens' Principle, Radiation Conditions, and Integral Formulas for the Scattering of Elastic Waves*, J. Acoust. Soc. Am. *59*, 1361–1371.

PEDERSEN, H. A., MAUPIN, V., and CAMPILLO, M. (1986), *Wave Diffraction in Multilayered Media with the Indirect Boundary Element Method: Application to 3-D Diffraction of Long-period Surface Waves by 2-D Lithospheric Structures*, Geophys. J. Int. *125*, 545–558.

PIESSENS, R., DONCKER-KAPENGA, E., ÜBERHUBER, C. W., and KAHANER, D. K., *QUADPACK: A Subroutine Package for Automatic Integration* (Springer-Verlag, Berlin 1983).

ROBERTS, R. A. (1994), *The Asymptotic Computational Ansatz: Application to Critical Angle Beam Transmission Boundary Integral Equation Solution*, J. Acoust. Soc. Am. *95* (4), 1711–1725.

SÁNCHEZ-SESMA, F. J., and CAMPILLO, M. (1991), *Diffraction of P, SV and Rayleigh Waves by Topographical Features: A Boundary Integral Formulation*, Bull. Seismol. Soc. Am. *81*, 2234–2253.

SCOTT, P., and HELMBERGER, D. (1983), *Applications of the Kirchhoff-Helmholtz Integral to Problems in Seismology*, Geophys. J. R. Astr. Soc. *72*, 237–254.

SINGH, S. C., and CHAPMAN, C. H. (1988), *WKBJ Seismogram Theory in Anisotropic Media*, J. Acoust. Soc. Am. *84* (2), 732–741.

STAMNES, J. J., SPJELKAVIK, B., and PEDERSEN, H. M. (1983), *Evaluation of Diffraction Integrals Using Local Phase and Amplitude Approximations*, Optica Acta *30*, 207–222.

TYGEL, M., SCHLEICHER, J., and HUBRAL, P. (1994), *Kirchhoff-Helmholtz Theory in Modelling and Migration*, J. Seismic Explor. *3*, 203–214.

WANG, X., and WALTHAM, D. (1995), *The Stable-beam Seismic Modelling Method*, Geophysical Prospecting *43*, 939–961.

WENZEL, F., STENZEL, K.-J., and ZIMMERMANN, U. (1990), *Wave Propagation in Laterally Heterogeneous Layered Media*, Geophys. J. Int. *103*, 675–684.

WHITE, J. E. (1982), *Computed Waveforms in Transversely Isotropic Media*, Geophysics *47*, 771–783.

WU, R.-S. (1985), *Gaussian Beams, Complex Rays, and Analytic Extension of the Green's Function in Smoothly Inhomogeneous Media*, Geophys. J. R. Astr. Soc. *83*, 93–110.

ZHU, T. (1988), *A Ray-Kirchhoff Method for Body-wave Calculations in Inhomogeneous Media: Theory*, Geophys. J. Int. *92*, 181–193.

(Received November 6, 1996, accepted July 15, 1997)